Lidija PETKOVSKA[1,2], Paul W. LEFLEY[3], Goga CVETKOVSKI[2]

International Balkan University Macedonia (1), Ss. Cyril and Methodius University of Skopje (2), University of Leicester (3)

Static Characteristics of a Novel Low Cost Brushless DC Permanent Magnet Motor

Abstract. *The paper presents the design attributes and static characteristics of a new 6/4 topology of a low cost brushless DC permanent magnet (BLDCPM) motor. To analyse the motor performance, steady state characteristics are obtained by using quasi-static finite element analysis (FEA). Computational results are presented in figures and tables. The analysis of the motor characteristics will be used as a reliable tool for design optimisation of this novel low cost BLDCPM motor.*

Streszczenie. *W artykule przedstawiono projekt nowego silnika bezszczotkowego DC z magnesami trwałymi w topologii 6/4. Do analizy właściwości silnika wykorzystano quasi-static metodę element skończonego. (**Właściwości statyczne nowego rodzaju silnika bezszczotkowego DC z magnesami trwałymi**).*

Keywords: Permanent Magnet Motor; Brushless Motor; FE Analysis; Design Optimisation.
Słowa kluczowe: in the case of foreign Authors in this line the Editor inserts Polish translation of keywords.

Introduction

Fractional-slot concentrated-winding synchronous PM motors have been gaining more interest over the last few years [1-5]. This is mainly due to the ease of manufacture at lower cost, as well as several advantages that this type of configuration provides, which mainly include: higher specific output power and torque density, higher efficiency, shorter end turns, high slot fill factor and lower cogging torque; also in addition, the flux-weakening capability and fault tolerance of the motor are significantly better.

In this motor topology the stator teeth are combined (slots are removed) to become large poles around which the concentrated windings are placed. This construction offers obvious advantages for electrical machines with radial air-gap, because the volume of copper used in the end-windings can be reduced in significant proportions. Furthermore, a significant reduction of the Joule losses is achieved, and the efficiency of the motor is improved when compared to more traditional structures.

In general, the concentrated-winding machines are divided in two major classes: single-layer and double-layer stator windings [1]. In the paper the authors present a development and analysis of three-phase surface-mounted permanent magnet motor with single-layer concentrated stator windings, which general view is presented in Fig. 1.

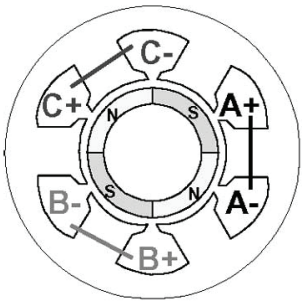

Fig.1. General structure of single-layer concentrated-winding

The objective of this work is to present a step-by-step building of a novel design for low-cost brushless DC permanent magnet (BLDCPM) motor. It is followed by development of an accurate nonlinear FEM model of the motor, including the rotor motion. A systematic method is proposed to determine the relevant motor characteristics by use of the field calculation software, and their performance analysis is discussed. This will help in the optimisation of the motor design, and will especially contribute for the minimisation of the cogging torque.

Motor Design Development

The authors have been investigating ways to bring down the manufacturing costs of electric motors by exploring interesting machine topologies [6]. This includes noninteger stator rotor pole ratios (known as fractional slot motors), and the use of asymmetrical stator pole arcs [7]. Fractional slot motors tend to have lower cogging torque than integer stator-rotor pole ratios, and for this reason it is decided to exploit this type of motor through further development. In the paper is presented a novel design of low cost 6/4 pole brushless DC permanent magnet (BLDCPM) motor, that has asymmetric stator pole arcs and a simple three phase winding in a star connection (Y).

The development of the BLDCPM motor design and its attributes are presented step-by-step. It is started from a simple four pole motor topology with surface mounted magnets; in twelve stator slots a three phase concentrated winding, with only one coil per phase and per pole pair, is inserted; the presentation is given in Fig. 2 (a). In the next step, one coil per phase is removed, whilst leaving three remaining coils of twice the number of turns; they are equally displaced around the stator core for 120^0. The new, now simplified initial topology is presented in Fig. 2 (b).

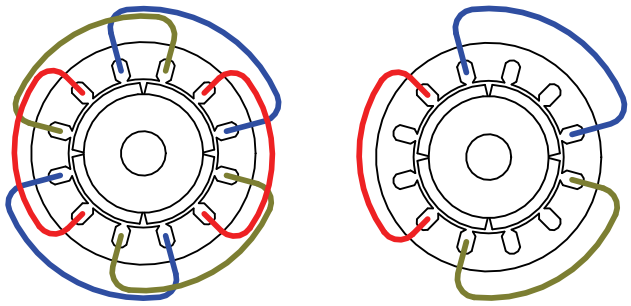

(a) (b)

Fig.2. Initial topology of 4-pole 12-slot motor

The stator punched zone can be further processed by removing the unused slots, and by increasing the remaining slot winding area; thus the stator core with asymmetric pole arcs will be derived. The three stator poles, carrying phase windings (large poles), have a pole arc X, while the three others (small poles) have a pole arc Y. The shoe thickness Z of the large pole is carefully designed to avoid high saturations in the pole tips. The design attributes of the BLDCPM are depicted in Fig. 3 (a). The novel 6/4 topology, upon which this paper is based, is presented more detailed in Fig. 3 (b).

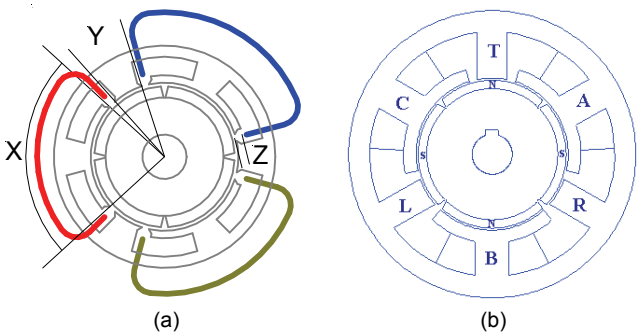

(a) (b)

Fig.3. Derivation of fractional slot 6/4 asymmetric PM motor

The three large poles, carrying the three phase windings, are labelled: phase A (2 o'clock), phase B (6 o'clock), and phase C (10 o'clock). The small poles, without windings, are used for smoothing the magnetic field distribution; they are labelled: Top pole T (12 o'clock), Right pole R (4 o'clock), and Left pole L (8 o'clock).

FE Model of the BLDCPM Motor

The field analysis of the BLDCPM motor is performed by using the 2D FEM code. As known, the magnetic field is prevailing in the interior of the machine. Hence, the domain of the solution Ω is bounded by two contours: outer contour D_1 and inner contour D_2. Accepting the 2D rectangular x-y plane system, the magnetostatic field problem is described in terms of the vector potential, and is obtained by solving the nonlinear Poisson equation:

$$(1) \qquad \begin{cases} \dfrac{\partial}{\partial x}\left(\nu_y \dfrac{\partial A_z}{\partial x}\right)+\dfrac{\partial}{\partial y}\left(\nu_x \dfrac{\partial A_z}{\partial y}\right)=-\left(J_z+J_m\right) \\ \mathbf{D_1}+\mathbf{D_2}: A_z=0 \end{cases}$$

where: A_z and J_z are the z-component of the vector potential **A** and current density **J**, respectively; J_m - is the equivalent current density of the PMs; ν_x and ν_y are the reluctivity components; $\mathbf{D_1}$ and $\mathbf{D_2}$ - denote Dirichlet boundaries (outer and inner contour of the domain $\mathbf{\Omega}$).

The Finite Element (FE) model of the motor and the field calculations are spread over the whole cross-section. All material properties are written in the input database. The initial position of the rotor, i.e. starting point 0 of the mid-gap circumference, against the reference stator axis is defined. The iron saturation and the cross-coupling between the PM flux and armature flux are taken into account. The FE model of the BLDCPM motor is shown in Fig. 4.

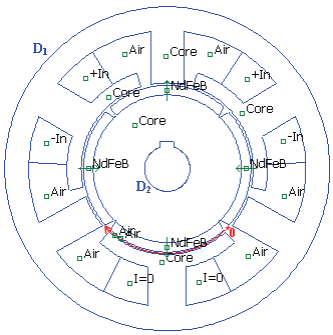

Fig.4. FE model of the BLDCPM motor

The pre-processor program has been used to implement the two dimensional finite element model of the motor. Firstly, the mesh of finite elements is generated over the whole motor cross section; it consists of about 40,000 nodes and 78,000 elements. A quarter of the mesh is given in Fig. 5 (a). To achieve a closer estimation of the motor performance, particular emphasis is put on increasing the mesh density in the air gap, as presented in Fig. 5 (b).

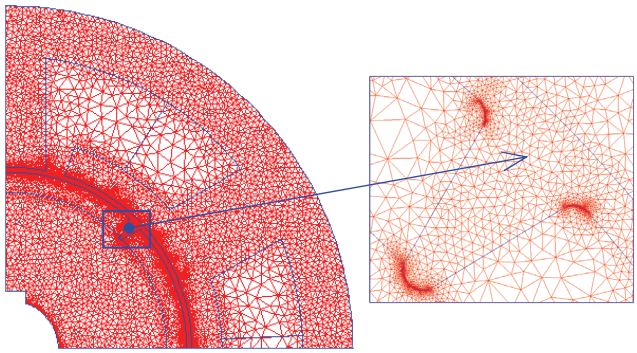

(a) across a quadrant (b) in the air-gap

Fig.5. FE Mesh of BLDCPM motor

Field analysis of the BLDCPM Motor

The analysis of the brushless DC permanent magnet motor performance starts with magnetostatic computation of the field distribution. The initial rotor position is taken as presented in Fig. 4, where the two N-poles of the rotor are aligned with B-phase axis of the large poles and T-pole axis of the small poles.

Retrieval of the magnetic field solution is made through the post-processing functions of the FEM software. First, the graphic display of the flux density contours is obtained. The visual presentation of the magnetic field under various operating stator currents is given in the next two figures.

The magnetic field distribution when the motor is unexcited, i.e. the stator current is set to 0, is shown in Fig. 6, where (a) presents the initial rotor position, whilst (b) shows the rotor displaced 90° in a clockwise direction. Fig. 7 (a) and (b) present the magnetic field distribution of the excited motor, at the rated current in the windings and for the same rotor positions. The excitation shown is for 120° conduction in each phase, where phase A is energised to present S-pole towards the air gap, phase C acts as N-pole, while phase B is unexcited.

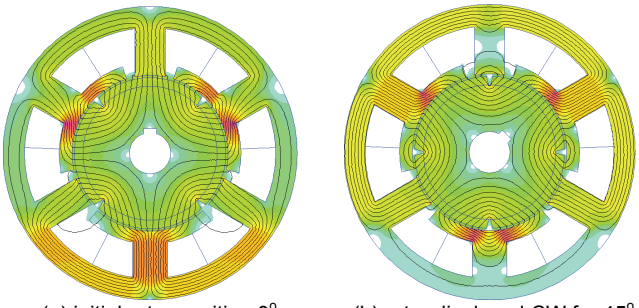

(a) initial rotor position 0° (b) rotor displaced CW for 45°

Fig.6. Magnetic flux distribution of unexcited BLDCPM motor

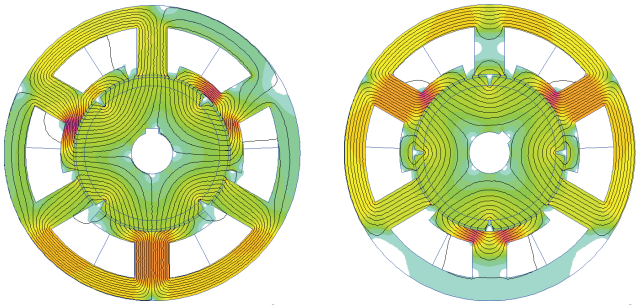

(a) initial rotor position 0° (b) rotor displaced CW for 45°

Fig.7. Magnetic flux distribution of the motor at rated current

Computational Results

The focus of the paper is to determine and present the FEM simulations of the steady state characteristics [8] of the new designed motor: air-gap flux excited by the PMs; magnetic flux density profile along the mid-gap line, flux linkages of the phase windings, induced back EMF, as well as electromagnetic torque and cogging torque. The motor characteristics are calculated and assessed at no-load and on-load by using a static FEA [9].

Flux Density Profile in the Air Gap

The air-gap magnetic field density provides valuable information in estimating motor performance. The knowledge of the flux density will not only allow an evaluation of the rated performance, but also a determination of such effects as cogging torque, ripple torque, back-emf, etc.

The common method for obtaining of the air gap flux density distribution along the mid-line of the air gap is in the post-processor of FEM software. For the same operating conditions from the previous section, illustrated in Fig. 6 (a) and Fig. 7 (a), the distribution of the radial component of magnetic flux density in the air gap is presented in Fig. 8 (a) and (b). The selected starting point is "0", as noted in Fig. 4; the motor is rotating in the clockwise (CW) direction.

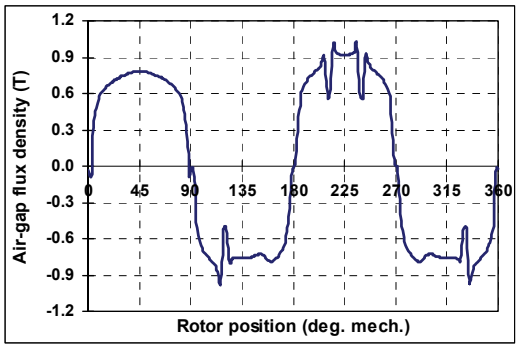

(a) zero current

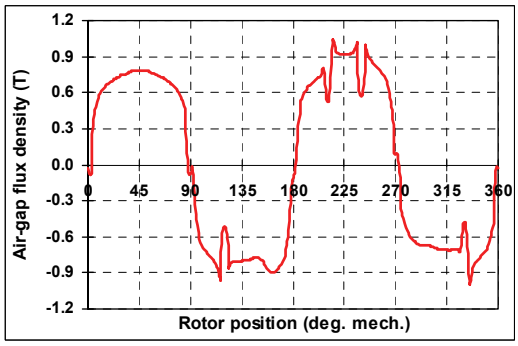

(b) rated current

Fig.8. Profile of the magnetic flux density in the air gap

Observing the previous figures, and comparing the characteristics when the motor operates without and with current in the phase windings, one can notice the effect of the stator field on the permanent magnets field.

Stator Pole Flux Profile

In the field theory, for closed and bounded systems, the numerical calculation of the magnetic flux can be performed by a number of equations, either when using values of the magnetic vector potential **A** along a contour, or magnetic flux density **B** over a surface. From calculated values for the magnetic vector potential in the analysed domain, and by using line integration of the FEM postprocessor along the mid-gap line, the characteristics of the fluxes, linked both to large and small poles, in dependence of the displacement angle θ, can be derived.

$$\Phi_g = \int_{\Sigma} \mathrm{rot}\boldsymbol{A} \cdot \mathrm{d}\boldsymbol{S} = \oint_{C} \boldsymbol{A} \cdot \mathrm{d}\,\boldsymbol{r} = \int_{\Sigma} \boldsymbol{B} \cdot \mathrm{d}\boldsymbol{S} \tag{2}$$

where: Σ is the surface area of the Dirichlet boundary; C is the length of integrating contour.

When only the field of the PMs exists, and for the large poles arc along the middle line of air-gap circumference, the fluxes Φ_A, Φ_B and Φ_C are determined; the characteristics are presented in Fig. 9. Similarly, taking arcs corresponding only to the small pole pitch, the fluxes Φ_T, Φ_R and Φ_L are obtained and presented in Fig. 10. Apart from the flux profile of a large stator pole which is close to a triangular wave with rounded tips, the profile of the small stator poles is quite flat; obviously, due to the shape of the pole shoes.

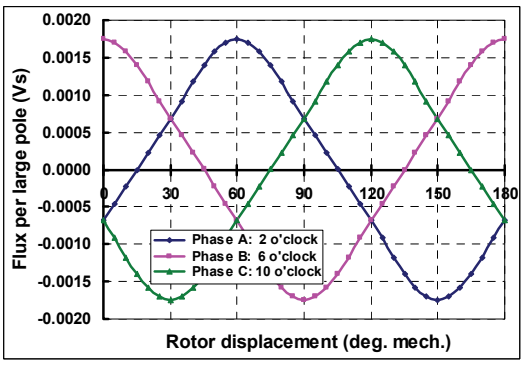

Fig.9. Magnetic flux of the large poles with no motor current

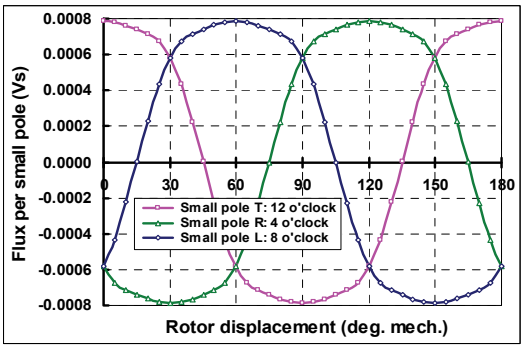

Fig.10. Magnetic flux of the small poles with no motor current

If we focus on the pole arc, corresponding to the stator C-phase, the characteristic $\Phi_C=f(\theta)$ at I=cons. is derived, and the influence of the stator field on the PMs can be analysed. The current in phase C acts in opposition to the rotor field, which offsets the flux with an average value different from zero; also, the physical neutral of the resultant field is bilaterally moved for approximately 5^o mech. For two typical values of the phase winding current, i.e. for zero and rated current, the predicted graphs are shown in Fig. 11.

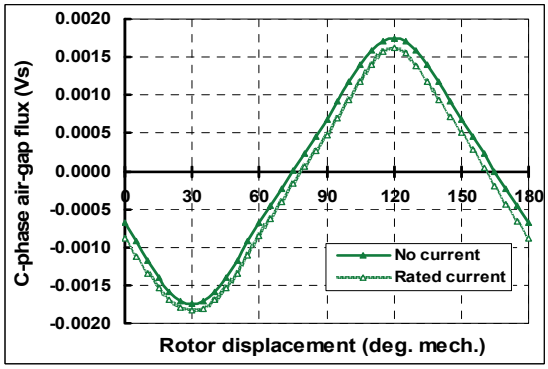

Fig.11. Magnetic flux of C-phase at zero and rated current

Flux Linkage and Back EMF

The *back-emf* is the voltage induced in the stator windings by the variable magnetic field in the air-gap. There are two common definitions of the back emf in literature. One definition treats the induced emf only as an effect of the rotor magnetic field change, while the other includes mutually and self-induced voltage between windings. In this study, the first definition is used. The flux linkage of stator windings, having N turns per pole and phase is:

$$\psi = N \cdot \phi \tag{3}$$

The expression for the calculation of the back EMF is derived from the function $\psi=f(\theta)$, obtained at stator current I=0; the developed procedure the authors have published in their previous works [6, 7]. The three phase-to-neutral back emf waveforms, at a speed of 1500 rpm, are shown in Fig. 12. One can notice a reasonably good trapezoidal shape, but significant influence of the 3rd harmonic component.

In the future, an improvement of the induced back-emf profile by designing the stator pole shoes/tips is anticipated. The authors have already presented similar results for a single-phase permanent magnet brushless DC motor [6].

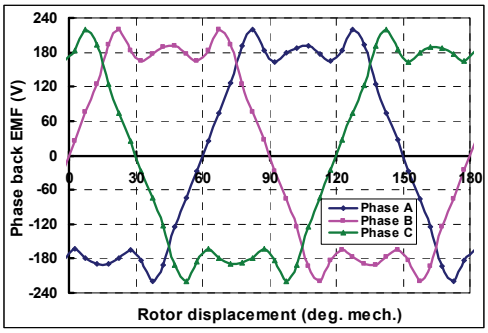

Fig.12. Phase-to-neutral back EMF profile at zero current

The line-to-line back-emf waveforms are presented in Fig. 13; these characteristics look smoother since the *triplen* harmonics cancel each other in their profile.

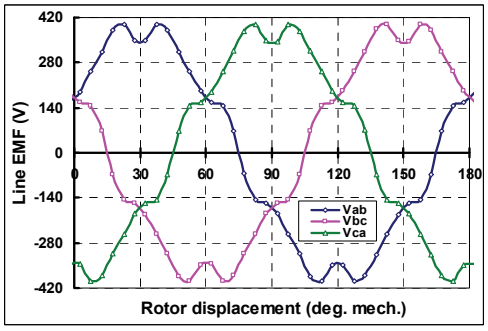

Fig.13. Line-to-line back EMF profile at zero current

Electromagnetic Torque

The knowledge of the static electromagnetic torque is very important for the performance analysis of electric motors. The torque in an electric motor can be calculated either analytically or numerically in a variety of ways.

Recently, many works have been published in this subject area. Although the attention is mostly put on analytical methods [2-5], the authors of the paper suggest the use of numerical finite element simulations [7, 9]. In general, they require global and local field solutions of very high accuracy, particularly for determination of the cogging torque. In other words, a high level of mesh discretisation is required in the finite element calculation; the particular emphasis to this issue was put previously (Fig.5 (b)), while developing the FE model of the BLDCPM motor.

The electromagnetic torque is computed by using the Weighted Stress Tensor (volume integral); two phases (A and C) are driven by two currents flowing in the opposite direction, whilst the third phase (B) remains open circuited. The series of simulations for a variety of stator currents and rotor displacement along one pole pitch are performed, and the dependence $T=f(I,\theta)$ is derived. Smooth and accurate prediction of the electromagnetic torque requires not only a high number of mesh elements in the air-gap, but also very small angle of the rotor displacement, often causing the computational time to become excessive.

The 3D surface of the predicted electromagnetic torque waveforms resulting from simultaneous change of armature current and rotor position are shown in Fig. 14.

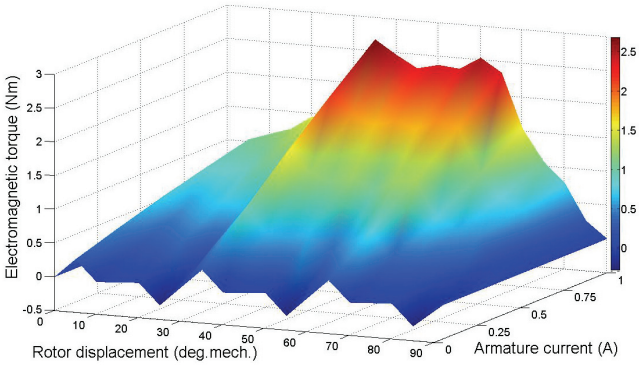

Fig.14. $T_{em}=f(I,\theta)$ in 3D presentation

Two other views, in two different planes Z-X and Z-Y, show two different sets of the same characteristics. From Fig. 15 comes into view the need for optimisation of the stator core geometry, and in particular the stator pole shoe, in order to improve the torque profile. In Fig. 16 it is evident that there is a linear dependence between the static torque and the armature current, which is in turn one of the main advantages of controlled PM motor drives.

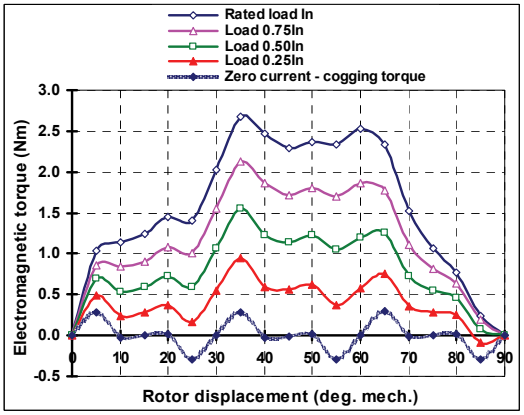

Fig.15. $T_{em}=f(\theta)$, I=cons. in Z-X plane

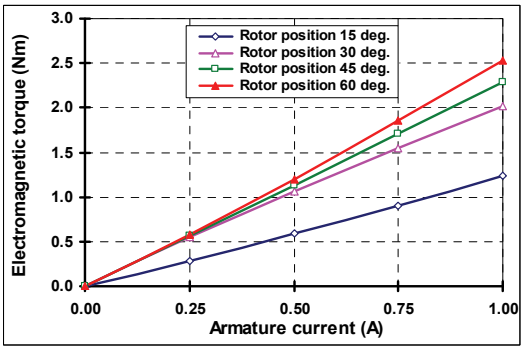

Fig.16. $T_{em}=f(I)$, θ=cons. in Z-Y plane

Cogging Torque

The cogging torque of PM motors is always a challenging matter for research and analysis [10]. Cogging torque in DC brushless PM motors comes from variations in magnetic field density around the rotor permanent magnets as they pass the non-uniform geometry of the stator. The pulsating speed of the rotor, that cogging usually generates, may cause significant levels of noise and vibrations.

Major factors affecting the cogging torque include PM magnetic field profile, air-gap length, stator openings, ratio of stator teeth and rotor poles, and skewing. In addition, copper fill, pole pitch, flux density or the flux distribution, magnet volume, and material weight can also influence both the peak value of the cogging and its profile.

Relationships between some of these factors are difficult to be defined. Consequently, the classical electromagnetic calculations do not provide either the data needed to determine accurately how much cogging torque might be developed in a motor, or the cogging profile.

A complete Finite Element Analysis (FEA) is an alternative method to be used, although it usually consumes more computational time. One period of the calculated cogging torque is presented in Fig. 17. The peak cogging torque is in the vicinity of 0.3 Nm, corresponding to approximately 11% of the peak electromagnetic torque; this fact initiates the need for reducing its value.

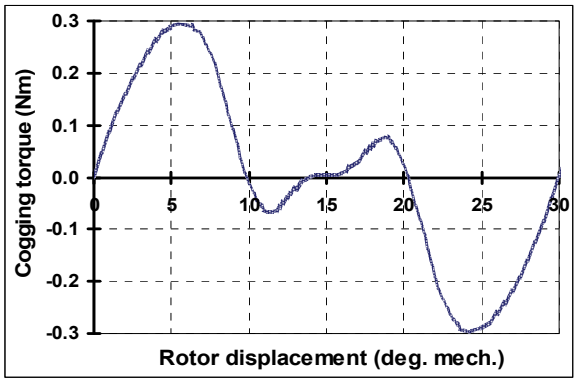

Fig.17. Cogging torque profile along one period (30^o mech.)

Conclusions

The prototype motor presented in this paper is a new structure of a surface mounted 6/4 PM motor, with fractional-slot concentrated windings, and asymmetric stator pole arcs. The notable features of this low cost motor are simple to manufacture, and an acceptable value of the cogging torque, resulting from the asymmetric stator poles and non-integer stator to rotor pole ratio.

The motor has been analysed by using FEM. The FE model provides a fast and reliable method to analyse the proposed motor design. The static characteristics of the brushless DC permanent magnet motor have been calculated; the results are presented in diagrams and thoroughly discussed. The magnetic field of the BLDCPM motor, analysed by 2D FEM, shows that the magnetic flux is mainly contributed by the PMs, while the stator field contributes little to the magnetic flux value, but changes the distribution of the resultant field.

The objective of this work is to develop an accurate nonlinear FE based model and to predict the steady state performance characteristics of the BLDCPM motor. This study demonstrates the utility and versatility of the FEM in the design procedure of new motor topologies. The validation of the results will be done through manufacturing an optimised prototype, and thus verifying the approach.

It is anticipated that industrial development of the presented design structure should increase in the near future and it should also not be restricted only to low power applications. The production process of the new proposed motor topology can be simplified by use of the new soft magnetic composites (SMC), which can further improve their manufacture and lower the production cost.

REFERENCES

[1] El-Refaie A. M., Fractional-Slot Concentrated-Windings Synchronous Permanent Magnet Machines: Opportunities and Challenges, *IEEE Transactions on Industrial Electronics*, 57 (2010), No. 1, 107-121.

[2] Wrobel R., Mellor P. H., Design Considerations of a Direct Drive Brushless Machine With Concentrated Windings, *IEEE Transactions on Energy Conversion*, 23 (2008), No. 1, 1-8.

[3] El-Refaie A. M., Jahns T. M., Novotny D. W., Analysis of Surface Permanent Magnet Machines With Fractional-Slot Concentrated Windings, *IEEE Transactions on Energy Conversion*, 21 (2006), No. 1, 34-43.

[4] Bianchi N., Bolognani S., Dai Pré M., Grezzani G., Design Considerations for Fractional-Slot Winding Configurations of Synchronous Machines, *IEEE Transactions on Industry Applications*, 42 (2006), No. 4, 997-1006.

[5] Cros J., Viarouge P. Synthesis of High Performance PM Motors With Concentrated Windings, *IEEE Transactions on Energy Conversion*, 12 (2002), No. 2, 248-253.

[6] Ahmed S., Lefley P. Development of a Single Phase PM BLDC Motor from a Novel Generic Model, *Proceedings of 11th Spanish Portuguese Conference on Electrical Engineering 11CHLIE* (2009), published on CD, pp. 1-5, Zaragoza, Spain.

[7] Lefley P., Petkovska L., Ahmed S., Cvetkovski G. Finite Element Analysis of a Novel Single Phase Permanent Magnet Brushless DC Motor, *Proceedings of 14th International Power Electronics and Motion Control Conference EPE-PEMC* (2010), published on CD, T4-96 – T4-101, Ohrid, Macedonia.

[8] Cheng M., Chau K. T., Chan C. C., Static Characteristics of a New Doubly Salient Permanent Magnet Motor, *IEEE Transactions on Energy Conversion*, 16 (2001), No. 1, 20-25.

[9] Petkovska L., Cvetkovski G., FEM Based Simulation of Permanent Magnet Synchronous Motor Performance Characteristics, *Proceedings of CES/IEEE 5th International Power Electronics and Motion Control Conference IPEMC* (2006), Vol. 1/3, 254-258, Shanghai, China.

[10] Ionel D. M., Popescu M., McGilp M. I., Miller T. J. E., Dellinger S. J., Assessment of Torque Components in Brushless Permanent Magnet Machines Through Numerical Analysis of the Electromagnetic Field, *IEEE Transactions on Industry Applications*, 42 (2005), No. 4, 1149-1158.

***Authors**: Prof. Dr Lidija Petkovska, Ss. Cyril and Methodius University, Faculty of Electrical Engineering and IT, P. O. Box 574, 1000 Skopje, Macedonia, e-mail: lidijap@feit.ukim.edu.mk ; Dr. Paul Lefley,* University of Leicester, Department of Engineering, University Road, Leicester, LE1 7RH, UK, e-mail: pwl3@leicester.ac.uk ; *Prof. Dr. Goga Cvetkovski, Ss. Cyril and Methodius University, Faculty of Electrical Engineering and IT, P. O. Box 574, 1000 Skopje, Macedonia, e-mail: gogacvet@feit.ukim.edu.mk .*

The Correspondence address is:
e-mail: lidijap@feit.ukim.edu.mk